Multiscale approach based predictions for shale rock's transversely isotropic properties considering the multi-inclusion and ITZ effects

Q. Chen * [a,b,c], M. Mousavi Nezhad [d], Q. Fisher [e] H.H, Zhu [b,c]

[a] *Key Laboratory of Advanced Civil Engineering Materials (Tongji University), Ministry of Education, 1239 Siping Road, Shanghai 200092, China*

[b] *Key Laboratory of Geotechnical and Underground Engineering of the Ministry of Education, Tongji University, 1239 Siping Road, Shanghai 200092, China*

[c] *State Key Laboratory for Disaster Reduction in Civil Engineering, Tongji University, 1239 Siping Road, Shanghai 200092, China*

[d] *Computational Mechanics, Civil Research Group, School of Engineering, University of Warwick, Warwick CV47AL, UK*

[e] *Centre for Integrated Petroleum Engineering and Geoscience, School of Earth and Environment, University of Leeds, Leeds, UK*

Abstract: Multiscale approach based explicit analytic predictions are obtained for the transversely isotropic properties of shale rock considering the multi-inclusion and *interfacial transition zone* (ITZ) effects. Representative volume elements (RVEs) are utilized to describe the material's hierarchical microstructures from the nanoscale to the macroscale. A new multilevel micromechanical homogenization scheme is presented to quantitatively estimate the material's transversely isotropic properties with the multi-inclusion and ITZ effects. The ITZ is characterized by the interphase material, whose effects are calculated by modifying the generalized self-consistent model. Furthermore, the explicit form solutions for the transversely isotropic properties are obtained by utilizing the Hill polarization tensor without numerical integration and the standard tensorial basis with the analytic inversions of fourth-rank tensors. To verify the proposed multiscale framework, predictions obtained via the proposed model are compared with experimental data and results estimated by the previous work, which show that the proposed multi-scaling approaches are capable of predicting the macroscopic behaviours of shale rocks with the multi-inclusion and ITZ effects. Finally, the influences of ITZ and inclusion properties on the material's macroscopic properties are discussed based on the proposed multiscale framework.

Keywords: multiscale modeling, multilevel micromechanical homogenizations, multi-inclusions, transversely isotropic properties, interfacial transition zone, shale rock.

* Corresponding author. E-mail: 13585546170@163.com

1 Introduction

Shale rock is especially critical for success of many fields of petroleum engineering and may also be important for the development of sustainable nuclear waste storage solutions [1,2].

Owing to the direct economic importance of shale rock, many efforts have been dedicated to model the material's mechanical properties, which can be mainly classified into two categories. The first category focuses on the empirical formulations to evaluate the properties of shale rock [3-8]. For examples, Dewhurst et al. presented the empirical strength prediction for preserved shales [3]; Farrokhrouz et al. proposed the empirical estimation of uniaxial compressive strength of shale formations [4]; Sayers used the clay-particle orientation distribution function to characterize shale elastic-anisotropy in dynamic measurements [5]. These formulations are obtained by means of laboratory or site tests, which is the phenomenological way to formulate the behavior of shale rock. The main limitation of such traditional approach is that it requires the extensive and costly experimental programs to characterize the material's properties. An attractive alternative to handle this kind of problem is provided by the framework of micromechanics, which reduces the laboratory expenses, meanwhile helps us throw light on the relations between the material's complicated microstructures and the macroscopic properties of shale rock [9-14]. For instances, Hornby et al. proposed a theoretical framework to predict the effective elastic properties of shale rocks based on the effective-medium method and found that the anisotropy of shale macroscopic elasticity was attributed to shape, orientation, and connection of the solid and fluid phase [9]. Giraud et al. used the Hill tensor to estimate the effective poroelastic properties of transversely isotropic rock-like composites [10]. Bobko et al. employed a strength homogenization approach to interpret the nanoindentation results and developed scaling relationships for indentation hardness with clay packing density [12]. Guo et al. presented a shale rock physics model for analysis of the brittleness index, mineralogy and porosity in Barnett shale [13].

Despite many attempts, progress in developing consistent micromechanics models that link mineralogy at the nanoscale to macroscopic properties of shale rock has been limited, due to the lack of

experimental data on the fundamental elastic properties of shale elementary building blocks, and links between those properties, morphology and macroscopic properties [15]. Recently, Ortega et al. proposed a multiscale framework to predict the transversely properties of shale rock with the self-consistent method and only the quartz inclusion is considered [15]. Actually there are many types of inclusions, such as quartz, calcite and dolomite, in the shale rock [9-14]. And the inclusions are not perfectly bonded to the matrix phase of shale rock, which implies that there are *interfacial transition zones* (ITZs) [16-19]. To address these issues, in this extension we propose a multiscale (from nanoscale to macroscale) predicting framework for the shale rock's transversely isotropic properties considering the multi-inclusion and ITZ effects with a new multilevel micromechanical homogenization scheme. Furthermore, in contrast with the composites containing isotropic phases, very few explicit analytical results can be found in literatures related to three-dimensional matrix composites with anisotropic components due to the significant mathematical difficulties appearing in such problems [20]. In our work, the standard tensorial basis [20] and the Hill polarization tensor without numerical integration [10] are modified to get the explicit form solutions for the transversely isotropic properties of the shale rock with multi-inclusion and ITZ effects.

The rest of this paper is organized as follows. The fundamentals of continuum micromechanics are introduced firstly in Section 2. Section 3 presents a multiscale model of shale rock based on the material's microstructures. In Section 4, new multilevel micromechanical homogenization procedures are proposed to estimate the effective transversely isotropic properties of shale rock. The ITZ effects are quantitatively considered by modifying the generalized self-consistent model. Furthermore, explicit form solutions for the effective transversely isotropic properties of shale rock are obtained by utilizing the Hill polarization tensor without numerical integration and the standard tensorial basis. Numerical examples including experimental validations and comparisons with existing micromechanical models are presented in Section 5, which also discusses the influences of multi-inclusions and ITZs on the

macroscopic properties of shale rock based on our proposed micromechanical framework. And some conclusions are reached in the final section.

2 Fundamentals of continuum micromechanics

2.1 The effective properties of the composite

One goal of continuum micromechanics is to estimate the effective elastic properties of the material defined over the representative volume element (RVE). The RVE is based on a 'mesoscopic' length scale, which is considerably larger than the characteristic length scale of particles (inhomogeneities) but smaller than the characteristic length scale of a macroscopic specimen [21]. Take a two-phase composite as an example, the effective elastic stiffness tensor C^* of the composite is defined through

$$\overline{\boldsymbol{\sigma}} = \mathbf{C}^* : \overline{\boldsymbol{\varepsilon}} \tag{1}$$

with

$$\overline{\boldsymbol{\sigma}} \equiv \frac{1}{V}\int_V \boldsymbol{\sigma}(\mathbf{x})d\mathbf{x} = \frac{1}{V}\left[\int_{V_0} \boldsymbol{\sigma}(\mathbf{x})d\mathbf{x} + \int_{V_1} \boldsymbol{\sigma}(\mathbf{x})d\mathbf{x}\right] \tag{2}$$

$$\overline{\boldsymbol{\varepsilon}} \equiv \frac{1}{V}\int_V \boldsymbol{\varepsilon}(\mathbf{x})d\mathbf{x} = \frac{1}{V}\left[\int_{V_0} \boldsymbol{\varepsilon}(\mathbf{x})d\mathbf{x} + \int_{V_1} \boldsymbol{\varepsilon}(\mathbf{x})d\mathbf{x}\right] \tag{3}$$

where V is the volume of an RVE, V_0 is the volume of the matrix, and V_1 is the volume of the inhomogeneity.

The effective elastic properties depend on the corresponding elastic moduli, the volume fraction of each constitute component, and the microstructures (e.g. the spatial distribution of the components) of the specific composite [22]. Due to the complex microstructures, many approximations instead of the exact solutions for these effective properties are developed in accordance with Eshelby's work [23-25].

2.2 The Eshelby solution and the polarization tensor

Eshelby derived the elastic field inside and outside an ellipsoidal inclusion in an infinite medium, and proposed the celebrated *equivalent inclusion principle* to relate the elastic inclusions and inhomogeneities [23-25]. The main theory behind the idea can be summarized as below: Let's consider an ellipsoid inhomogeneity (particle with properties different from those of the homogeneous matrix) embedded in an infinite matrix. According to Eshelby's equivalence principle, the perturbed strain field $\boldsymbol{\varepsilon}'(\mathbf{x})$ induced by inhomogeneity can be related to specified eigenstrain $\boldsymbol{\varepsilon}^*(\mathbf{x})$ by replacing the inhomogeneity with the matrix material (or vice versa). That is, for the domain of the inhomogeneity with elastic stiffness tensor $\mathbf{C}_1$, we have

$$\mathbf{C}_1 : \left[\boldsymbol{\varepsilon}^0 + \boldsymbol{\varepsilon}'(\mathbf{x})\right] = \mathbf{C}_0 : \left[\boldsymbol{\varepsilon}^0 + \boldsymbol{\varepsilon}'(\mathbf{x}) - \boldsymbol{\varepsilon}^*(\mathbf{x})\right] \tag{4}$$

with

$$\boldsymbol{\varepsilon}'(\mathbf{x}) = \mathbf{S} : \boldsymbol{\varepsilon}^*(\mathbf{x}) \tag{5}$$

where $\boldsymbol{\varepsilon}^0$ is the uniform strain field induced by far-field loads for a homogeneous matrix material only. $\mathbf{S}$ is the Eshelby tensor associated with the inhomogeneity, which can be represented by the Hill polarization tensor $\mathbf{P}$ as $\mathbf{S} = \mathbf{P} : \mathbf{C}_0$, and $\mathbf{C}_0$ and $\mathbf{C}_1$ are the stiffness tensors of the matrix and the inhomogeneity. For details see [26].

For a real material, there are usually many different inhomogeneities in the RVE. Therefore, it is difficult to obtain the exact perturbed strain field due to so many randomly distributed inhomogeneities that influence each other. Through making a set of assumptions, different micromechanical methods such as the Mori-Tanaka method [27,28], the self-consistent method [29] and Ju's method [21,34-38] have been derived based on the Eshelby solutions to estimate the effective properties of heterogeneous materials.

3 Multiscale representation of hierarchical structures of shale rock

3.1 Hierarchical structures of shale rock

Shale rocks are heterogeneous in nature and generally consist of different constituents or phases, such as clay material, quartz and calcite. Further, the constituents of materials can be treated as homogeneous at a certain length scale, but when observed at a smaller length scale, the constituents themselves may become heterogeneous, i.e. a multiscale phenomenon for heterogeneous shale rock materials [9-15]. According to [13], the components of shale rocks should include clays, kerogen, cracks, pores, quartz, calcite and dolomite. The rock properties are dependent on the microstructure parameters such as the orientation of clay platelets and cracks, pore/crack connectivity and shale mineralogical composition, including quartz, calcite and dolomite [11]. There are many other researches that characterize the microstructures and properties of shale rock at different length scales [30-33].

3.2 Multiscale models of shale materials

Due to these heterogeneous and multiscale natures, it is usually impractical and often impossible to describe all the precise characters of the microstructure of shale rocks. To characterize the material's heterogeneous and multiscale features, a new multiscale model is proposed based on [2] to represent the hierarchical and heterogeneous structures of shale rock by taking multi-inclusions, such as quartz, calcite and dolomite, and the ITZs into considerations, as exhibited in **Fig. 1.**

Similar with [2], the fundamental scale of shale materials is assumed to be the scale of elementary clay particles, which can be defined by scale '0'; at scale 'I', the material can be seen as porous clay composite. The characteristic size of scale 'II' is in the sub-millimeter and millimeter range, and the material is composed of porous clay fabric intermixed with an abundant population of poorly sorted detrital grains. The multi-inclusions and their ITZs are considered at this scale. The shale rocks are represented by homogenous material at the macroscopic scale, denoted by scale 'III'. On the basis of

this multiscale model, the macroscopic properties at scale 'III' of the shale materials can be characterized by the microstructures at lower length scales.

4 Multilevel homogenization approach for estimating the effective properties of shale rock

4.1 Multilevel homogenization schemes for shale rock

Based on the previous works [34-49], a new multilevel micromechanical homogenization framework is proposed to quantitatively estimate the transversely isotropic properties of shale rock with multi-inclusion and ITZ effects, as displayed in **Fig. 2.** Specifically, the first equivalent matrix made up of the pores and clay particles are reached with the first level homogenization, as exhibited in **Fig.2.a**. The ITZ effects are taken into consideration by the second level homogenization as shown by **Fig.2.b**, through which different types of equivalent inclusions are obtained when different silt inclusions, such as quartz, calcite and dolomite, are considered. By adding the different types of equivalent inclusions into the equivalent matrix step by step, the effective properties of the (1+*i*)th equivalent matrix and shale rock can be calculated by the (2+*i*)th and (2+*n*)th level homogenizations, respectively, as displayed in **Fig.2.c**. Here i = 1,2…n, which represents the type of the silt inclusion. n means the sum of all silt inclusion types.

4.2 Properties of the porous clay composite

According to [50,51], when a two-phase composite is considered, the effective elastic stiffness tensor can be reached as follows:

$$\sum_{r=1}^{2} c_r \left(\left(\mathbf{C}^r - \mathbf{C}^* \right)^{-1} + \mathbf{P}^r \right)^{-1} = 0 \tag{6}$$

Where c_r and $\mathbf{C}^r$ is respectively the volume fraction and the stiffness tensor of the rth component (including the matrix phase and the inclusion phase; here different phases mean materials with different

physical properties); $\mathbf{C}^*$ is the effective stiffness tensor of the two-phase composite; and $\mathbf{P}^r$ is the Hill polarization tensor, which can be expressed via the known Eshelby tensor. For details, see [26].

Let's define $\mathbf{C}_p$ and $\mathbf{C}_c$ as the stiffness tensors of the pores and clay particles, respectively. $\mathbf{C}_{e1}$ signifies the effective stiffness tensor of porous clay composite, which is the first equivalent matrix in our paper. The effective properties of the porous composite can be reached according to Eq.(6):

$$c_p\left(\left(\mathbf{C}_p-\mathbf{C}_{e1}\right)^{-1}+\mathbf{P}^p\right)^{-1}+c_c\left(\left(\mathbf{C}_c-\mathbf{C}_{e1}\right)^{-1}+\mathbf{P}^c\right)^{-1}=0 \tag{7}$$

$$c_p=\frac{V_p}{V_p+V_c};\quad c_c=\frac{V_c}{V_c+V_p} \tag{8}$$

Where c_p and c_c are respectively the volume fraction of the micro-pores and clay particles; V_p and V_c ($\mathbf{P}^p$ and $\mathbf{P}^c$) are the volume (Hill polarization tensors) of the micropores and clay particles, respectively.

4.3 Properties of the equivalent inclusions with the ITZs

Take the calcite inclusion as an example. There are ITZs between the calcites and the porous clay composite. Let Δ signify the thickness of ITZ and r represent the radius of the calcite inclusion. For simplification, the ratio of $r/(r+\Delta)$ for each calcite is supposed to be constant. To quantitatively calculate the ITZ influence on the equivalent inclusion's properties, the three-phase model proposed by Christensen and Lo [52], known as the generalized self-consistent model, is employed by modifying its inner- and outer-layer phases into the calcite inclusion and the ITZ, respectively. Accordingly, the effective bulk modulus and shear modulus for the equivalent inclusion can be expressed as follows:

$$K_{eca}=K_{it1}+\frac{\phi_1(K_{ca}-K_{it1})(3K_{it1}+4\mu_{it1})}{3K_{it1}+4\mu_{it1}+3(1-\phi_1)(K_{ca}-K_{it1})} \tag{9}$$

$$A\left(\frac{\mu_{eca}}{\mu_{it1}}\right)^2+B\left(\frac{\mu_{eca}}{\mu_{it1}}\right)+C=0 \tag{10}$$

where

$$A = 8\left[\frac{\mu_{ca}}{\mu_{it1}} - 1\right](4 - 5\nu_2)\eta_\alpha\ \phi_1^{10/3} - 2\left[63\left(\frac{\mu_{ca}}{\mu_{it1}} - 1\right)\eta_\beta + 2\eta_\alpha\eta_\gamma\right]\phi_1^{7/3}$$
$$+252\left[\frac{\mu_{ca}}{\mu_{it1}} - 1\right]\eta_\beta\,\phi_1^{5/3} - 50\left[\frac{\mu_{ca}}{\mu_{it1}} - 1\right](7 - 12\nu_{it1} + 8\nu_{it1}^{\ 2})\eta_\beta\,\phi_1 + 4(7 - 10\nu_{it1})\eta_\beta\,\eta_\gamma \quad (11)$$

$$B = -4\left[\frac{\mu_{ca}}{\mu_{it1}} - 1\right](1 - 5\nu_{it1})\eta_\alpha\ \phi_1^{10/3} + 4\left[63(\frac{\mu_{ca}}{\mu_{it1}} - 1)\eta_\beta + 2\eta_\alpha\eta_\gamma\right]\phi_1^{7/3}$$
$$-504\left[\frac{\mu_{ca}}{\mu_{it1}} - 1\right]\eta_\beta\ \phi_1^{5/3} + 150\left[\frac{\mu_{ca}}{\mu_{it1}} - 1\right](3 - \nu_{it1})\nu_{it1}\eta_\beta\,\phi_1 + 3(15\nu_{it1} - 7)\eta_\beta\ \eta_\gamma \quad (12)$$

$$C = 4\left[\frac{\mu_{ca}}{\mu_{it1}} - 1\right](5\nu_{it1} - 7)\eta_\alpha\,\phi_1^{10/3} - 2\left[63(\frac{\mu_{ca}}{\mu_{it1}} - 1)\eta_\beta + 2\eta_\alpha\eta_\gamma\right]\phi_1^{7/3}$$
$$+252\left[\frac{\mu_{ca}}{\mu_{it1}} - 1\right]\eta_\beta\ \phi_1^{5/3} + 25\left[\frac{\mu_{ca}}{\mu_{it1}} - 1\right](\nu_{it1}^{\ 2} - 7)\eta_\beta\,\phi_1 - 3(7 + 5\nu_{it1})\eta_\beta\,\eta_\gamma \quad (13)$$

with

$$\eta_\alpha = \left[\frac{\mu_{ca}}{\mu_{it1}} - 1\right](49 - 50\nu_{ca}\,\nu_{it1}) + 35\left(\frac{\mu_{ca}}{\mu_{it1}}\right)(\nu_{ca} - 2\nu_{it1}) + 35(2\nu_{ca} - \nu_{it1}) \quad (14)$$

$$\eta_\beta = 5\nu_{ca}\left[\frac{\mu_{ca}}{\mu_{it1}} - 8\right] + 7\left[\frac{\mu_{ca}}{\mu_{it1}} + 4\right] \quad (15)$$

$$\eta_\gamma = \frac{\mu_{ca}}{\mu_{it1}}[8 - 10\nu_{it1}] + (7 - 5\nu_{it1}) \quad (16)$$

$$\phi_1 = \left(\frac{r}{r + \Delta}\right)^3 \quad (17)$$

where ϕ_1 is the volume fraction of the calcite phase in the two-phase composite composed of the calcite and the ITZ. K_{ca}, μ_{ca} and ν_{ca} (K_{it1}, μ_{it1} and ν_{it1}) are bulk modulus, shear modulus and Poisson's ratio for the calcite (the ITZ), respectively. K_{eca} and μ_{eca} are the bulk modulus and shear modulus for the equivalent calcite inclusion, respectively. Similar homogenization procedures can be performed to take the other inclusions' ITZs into consideration.

4.4 Properties of shale rock with multi-inclusion and ITZ effects

In this section, three different types of silt inclusions are taken as examples to illustrate our proposed multilevel homogenization scheme. Let $\mathbf{C}_{eq}$, $\mathbf{C}_{eca}$ and $\mathbf{C}_{ed}$ respectively represent the stiffness tensor of the equivalent inclusion for quartz, calcite and dolomite.

Firstly, take the quartz and its ITZ as the first type of inclusion in the first equivalent matrix. According to [50,51], the properties of the second equivalent matrix composed by the first equivalent matrix obtained after the first level homogenization and the equivalent quartz inclusion(made up of the quartz and its ITZ) calculated by the second level homogenization can be reached by the following expression

$$c_{eq}\left(\left(\mathbf{C}_{eq}-\mathbf{C}_{e2}\right)^{-1}+\mathbf{P}^{eq}\right)^{-1}+c_{e1}\left(\left(\mathbf{C}_{e1}-\mathbf{C}_{e2}\right)^{-1}+\mathbf{P}^{e1}\right)^{-1}=0 \tag{18}$$

with

$$c_{eq}=\frac{V_{eq}}{V_{eq}+V_{e1}};\quad c_{e1}=\frac{V_{e1}}{V_{eq}+V_{e1}};\quad V_{eq}=V_q+V_{qITZ};\quad V_{e1}=V_p+V_c \tag{19}$$

where c_{eq} and c_{e1} are respectively the volume fraction of the equivalent quartz inclusion and porous composite; V_{eq} and V_{e1} ($\mathbf{P}^{eq}$ and $\mathbf{P}^{e1}$) are the volume(Hill polarization tensor) of the equivalent quartz inclusion and porous composite, respectively; $\mathbf{C}_{e2}$ is the effective stiffness tensor of the second equivalent matrix, V_q and V_{qITZ} is the volume of quartz inclusions and their ITZs.

Secondly, when the calcite inclusion is added, the effective properties of the composite made up of the porous composite, the quartz, calcite and their ITZs can be obtained by

$$c_{ec}\left(\left(\mathbf{C}_{ec}-\mathbf{C}_{e3}\right)^{-1}+\mathbf{P}^{ec}\right)^{-1}+c_{e2}\left(\left(\mathbf{C}_{e2}-\mathbf{C}_{e3}\right)^{-1}+\mathbf{P}^{e2}\right)^{-1}=0 \tag{20}$$

with

$$c_{ec} = \frac{V_{ca} + V_{caITZ}}{V_p + V_c + V_q + V_{qITZ} + V_{ca} + V_{caITZ}} \qquad c_{e2} = \frac{V_p + V_c + V_q + V_{qITZ}}{V_p + V_c + V_q + V_{qITZ} + V_{ca} + V_{caITZ}} \tag{21}$$

where c_{ec} and c_{e2} ($\mathbf{P}^{ec}$ and $\mathbf{P}^{e2}$) are respectively the volume fraction (Hill polarization tensor) of the equivalent calcite inclusion and the second equivalent matrix; $\mathbf{C}_{e3}$ is the effective stiffness tensor of the third equivalent matrix, V_{ca} and V_{caITZ} are the volume of calcite inclusions and their ITZs.

Thirdly, the properties of the composite consisting of the porous composite, the quartz, the calcite, the dolomite and their ITZs can be calculated with the third equivalent matrix, which can be expressed as follows:

$$c_{ed}\left(\left(\mathbf{C}_{ed} - \mathbf{C}_{e4}\right)^{-1} + \mathbf{P}^{ed}\right)^{-1} + c_{e3}\left(\left(\mathbf{C}_{e3} - \mathbf{C}_{e4}\right)^{-1} + \mathbf{P}^{e3}\right)^{-1} = 0 \tag{22}$$

with

$$c_{ed} = \frac{V_d + V_{dITZ}}{V_p + V_c + V_q + V_{qITZ} + V_{ca} + V_{caITZ} + V_d + V_{dITZ}} \qquad c_{e3} = \frac{V_p + V_c + V_q + V_{qITZ} + V_{ca} + V_{caITZ}}{V_p + V_c + V_q + V_{qITZ} + V_{ca} + V_{caITZ} + V_d + V_{dITZ}} \tag{23}$$

where c_{ed} and c_{e3} ($\mathbf{P}^{ed}$ and $\mathbf{P}^{e3}$) are respectively the volume fraction (Hill polarization tensor) of the equivalent dolomite inclusion and the third equivalent matrix; respectively; $\mathbf{C}_{e4}$ is the effective stiffness tensor of the forth equivalent matrix, V_d and V_{dITZ} are the volume of dolomite inclusion and its ITZ.

As for the other kinds of inclusions, the multilevel homogenization scheme can be similarly applied. If no other silt inclusions are taken into consideration, $\mathbf{C}_{e4}$ will be the effective stiffness tensor for the shale rock with the multi-inclusion and ITZ effects.

4.5 The explicit form solutions for the effective properties with the ITZ

According to [2], the transversely isotropic properties of shale rock are mainly due to the transversely isotropic properties of the clay particles at nanoscale. For the transversely isotropic matrix or inclusions, the solutions for the micromechanical equations, like Eq. (6), become much more complex

than isotropic materials [10,14,20]. For easy applications, the following mathematical treatments are utilized to obtain the explicit form solutions for the effective transversely isotropic properties of shale rock.

On the one hand, the method provided by Giraud et al. [10] is utilized to obtain the Hill polarization tensor **P** for the spherical inclusion in a transversely isotropic solid. This method is based on the analytical expressions of Eshelby's tensor **S** developed by Withers [53] and the relations between these two tensors [10]. The components of the tensor **P** for a transversely isotropic medium can be calculated based on the following expressions [10]:

If $C_{13}^{*}-C_{13}-2C_{44}\neq 0$,

$$\begin{aligned}
&P_{11}=\frac{3}{2}\sum_{i=1}^{2}\nu_i A_i' I_1(i)+\frac{DI_1(3)}{4},\quad P_{12}=\frac{1}{2}\sum_{i=1}^{2}\nu_i A_i' I_1(i)-\frac{DI_1(3)}{4}\\
&P_{13}=\sum_{i=1}^{2}k_i\nu_i^3 A_i' I_2(i),\quad P_{33}=-2\sum_{i=1}^{2}k_i^2\nu_i^5 A_i' I_2(i)\\
&P_{44}=\frac{1}{4}\sum_{i=1}^{2}(1+k_i)\nu_i^3 A_i'\left[I_2(i)-2k_i I_1(i)\right]+\frac{D\nu_3^2 I_2(3)}{8}
\end{aligned}\tag{24}$$

with

$$\begin{aligned}
&A_i=-B_i,\ A_i'=B_i',\quad A_i=-2\nu_i k_i A_i',\quad \nu_1 A_1=-\nu_2 A_2=\frac{C_{13}+C_{44}}{4\pi\left(\nu_2^2-\nu_1^2\right)C_{33}C_{44}}\\
&A_1'=\frac{C_{44}-\nu_1^2 C_{33}}{8\pi\left(\nu_2^2-\nu_1^2\right)\nu_1^2 C_{33}C_{44}},\qquad A_2'=\frac{C_{44}-\nu_2^2 C_{33}}{8\pi\left(\nu_2^2-\nu_1^2\right)\nu_2^2 C_{33}C_{44}}
\end{aligned}\tag{25}$$

If $C_{13}^{*}-C_{13}-2C_{44}=0$,

$$\begin{aligned}
&P_{11}=3\left(\frac{C_{13}}{C_{13}+C_{44}}\right)B_1 I_1(1)-6B_1 I_{12}+\frac{D}{4}I_1(3),\quad P_{12}=\left(\frac{C_{13}}{C_{13}+C_{44}}\right)B_1 I_1(1)-2B_1 I_{12}-\frac{D}{4}I_1(3)\\
&P_{13}=2B_1\left[-3I_1(1)+\nu_1^2 I_2(1)+4I_{12}\right],\quad P_{33}=4\nu_1^2 B_1\left[3I_1(1)-\left(\frac{C_{11}}{C_{13}+C_{44}}\right)I_2(1)-4I_{12}\right]\\
&P_{44}=-B_1\left[3+\nu_1^2\left(3+\frac{C_{44}}{C_{13}+C_{44}}\right)\right]I_1(1)+\frac{B_1\nu_1^2}{2}\left(\frac{C_{13}}{C_{13}+C_{44}}\right)I_2(1)+4B_1\left(1+\nu_1^2\right)I_{12}+\frac{D}{8}\nu_3^2 I_2(3)
\end{aligned}\tag{26}$$

with

$$\nu_1=\nu_2=\left(C_{11}/C_{33}\right)^{\frac{1}{4}},\quad k_1=k_2=1,\quad R_1=R_2,\quad B_1=B_2=-\nu_1\frac{C_{13}+C_{44}}{16\pi C_{11}C_{44}}$$
$$A_1'=-A_2'=\frac{1}{16\pi C_{11}}=-B_1\frac{C_{44}}{\nu_1\left(C_{13}+C_{44}\right)},\quad B_1'=B_2'=\frac{1}{16\pi C_{44}\nu_1^2}=-B_1\frac{C_{11}}{\nu_1^3\left(C_{13}+C_{44}\right)} \tag{27}$$

where

$$C_{13}^*=\left(C_{11}C_{33}\right)^{\frac{1}{2}},\quad k_i=\frac{C_{11}/\nu_i^2-C_{44}}{C_{13}+C_{44}},\quad D=\frac{1}{4\pi C_{44}\nu_3},\quad \nu_3=\left(\frac{C_{66}}{C_{44}}\right)^{\frac{1}{2}}$$
$$\nu_1=\left[\frac{\left(C_{13}^*-C_{13}\right)\left(C_{13}^*+C_{13}+2C_{44}\right)}{4C_{33}C_{44}}\right]^{\frac{1}{2}}+\left[\frac{\left(C_{13}^*+C_{13}\right)\left(C_{13}^*-C_{13}-2C_{44}\right)}{4C_{33}C_{44}}\right]^{\frac{1}{2}} \tag{28}$$
$$\nu_2=\left[\frac{\left(C_{13}^*-C_{13}\right)\left(C_{13}^*+C_{13}+2C_{44}\right)}{4C_{33}C_{44}}\right]^{\frac{1}{2}}-\left[\frac{\left(C_{13}^*+C_{13}\right)\left(C_{13}^*-C_{13}-2C_{44}\right)}{4C_{33}C_{44}}\right]^{\frac{1}{2}}$$

where C_{11}, C_{12}, C_{13}, C_{33}, C_{44} and C_{66} are the components of the stiffness tensor of the transversely isotropic medium, and the explicit expressions for $I_1(i), I_2(i)$ and I_{12} can be found in [10].

On the other hand, the special tensor basis **T** [14] is employed to simplify the fourth-rank tensors calculations. The operations of analytic inversion and multiplication of fourth-rank tensors are conveniently done with this tensor basis. See **Appendix A** for details.

With the solution of the Hill polarization tensor **P** and tensor basis **T**, Eqs. (29)–(36) can be obtained by equating each component to zero in Eq. (6) as follows:

$$\sum_{r=1}^{2}c_r\left(\frac{\left(C_{11}^r+C_{12}^r-C_{11}^*-C_{12}^*\right)/\Delta_1^r+P_6^{*r}}{\Delta_2^r}\right)=0 \tag{29}$$

$$\sum_{r=1}^{2}c_r\left(\frac{1}{2\left(C_{66}^r-C_{66}^*\right)}+P_2^{*r}\right)^{-1}=0 \tag{30}$$

$$\sum_{r=1}^{2}c_r\left(\frac{\left(C_{13}^r-C_{13}^*\right)/\Delta_1^r-P_3^{*r}}{\Delta_2^r}\right)=0 \tag{31}$$

$$\sum_{r=1}^{2} c_r \left(\frac{1}{\left(C_{44}^r - C_{44}^* \right)} + P_5^{*r} \right)^{-1} = 0 \tag{32}$$

$$\sum_{r=1}^{2} c_r \left(\frac{\left(C_{33}^r - C_{33}^* \right) / 2\Delta_1^r + P_1^{*r}}{\Delta_2^r} \right) = 0 \tag{33}$$

with

$$\Delta_1^r = \left(C_{11}^r + C_{12}^r - C_{11}^* - C_{12}^* \right) \left(C_{33}^r - C_{33}^* \right) - 2 \left(C_{13}^r - C_{13}^* \right)^2 \tag{34}$$

$$\Delta_2^r = 2 \left(\left(\frac{\left(C_{33}^r - C_{33}^* \right)}{2\Delta_1^r} + P_1^{*r} \right) \left(\frac{\left(C_{11}^r + C_{12}^r - C_{11}^* - C_{12}^* \right)}{\Delta_1^r} + P_6^{*r} \right) - \left(\frac{\left(C_{13}^r - C_{13}^* \right)}{\Delta_1^r} - P_4^{*r} \right)^2 \right) \tag{35}$$

$$P_1^{*r} = \left(P_{11}^{*r} + P_{12}^{*r} \right) / 2, \;\; P_2^{*r} = 2P_{66}^{*r} = P_{11}^{*r} - P_{12}^{*r}, \;\; P_3^{*r} = P_4^{*r} = P_{13}^{*r}, \;\; P_5 = 4P_{44}^{*r}, \;\; P_6^r = P_{33}^{*r} \tag{36}$$

where C_{11}^r, C_{12}^r, C_{13}^r, C_{33}^r, C_{44}^r and C_{66}^r are the components of the stiffness tensor of the *r*th phase in the transversely isotropic medium, C_{11}^*, C_{12}^*, C_{13}^*, C_{33}^*, C_{44}^* and C_{66}^* are the components of the stiffness tensor of the homogenized transversely isotropic media; and P_{11}^{*r}, P_{12}^{*r}, P_{13}^{*r}, P_{33}^{*r}, P_{44}^{*r} and P_{66}^{*r} are the components of the Hill polarization tensor of the *r*th phase in the homogenized transversely isotropic media. The other micromechanical equations, such as Eqs.(7) ,(18), (20) and (22) can be similarly solved.

5 Verification and discussions

5.1 Comparison with the existing results

Both the experimental data [15] and the existing estimations [14] are employed to verify our proposed multiscale framework. The model parameters of [15] are utilized as the input, and are composed of the material properties of the elementary phases present in shale rocks, including the five independent constants of the clay particle and the elastic properties of quartz. Since there are few experimental data available for the authors on the ITZ between the quartz and the porous composite,

three different types of ITZ parameters, as shown in Table 1, are employed as examples to verify the capacity of our proposed multiscale framework.

Fig. 3(a) shows comparisons among our predicting results, the experimental data of specimen G-01 [15] and results obtained by [14]. It can be found that our predicting results are the same as those of [14] when the ITZ properties are the same as those of the inclusions. Furthermore, it can be seen that the estimations correspond better with the experimental data by considering the ITZ effects. Similar conclusions can be reached when other specimens are employed as comparisons. See details in **Figs.3(b)–(c)**.

Through the comparisons with the experimental data and the results obtained by the existing models, it can be verified that our proposed multiscale framework, including the multiscale representations for the material's microstructures, multilevel homogenization scheme and the explicit form solutions for the transversely isotropic properties, is both feasible and capable of predicting the mechanical performance of shale rock with the ITZs.

5.2 Discussion on the influence of the ITZs

The properties of shale rock are influenced by the ITZs. It should be noted that the exact values for ITZ thicknesses and properties are not discussed in this section. Here, we focus on the quantitative influence of the specified ITZ thicknesses and properties on the material's macroscopic properties. As in Section 5.1, only the quartz inclusion is considered and three types of ITZs are employed as examples to illustrate the quantitative influence of the properties of the ITZs upon the mechanical performance of the shale rocks. The properties of the three types of ITZs are listed in Table 1. With the change of the ITZs, the properties of the shale rock will vary accordingly.

Figs. 4(a)–(b) present the variations in the mechanical properties of the equivalent inclusion composed of the ITZ and quartz inclusion with the increasing volume fraction of the ITZ. It can be seen that the properties of the equivalent inclusion gradually decrease when the ITZ has a lower bulk

modulus and shear modulus. When the properties of the ITZ are the same as those of the quartz, implying the perfect bonding, the properties of the equivalent inclusions remain constant. This result is reasonable in that there are no ITZ effects when the ITZ has the same performance as the quartz inclusions.

Figs. 5(a)–(b) display the variations in the components of the shale rock's stiffness tensor with different ITZs. It can be seen that the values of the stiffness tensor become smaller when the ITZ is not as strong as the quartz inclusions with the increase of the ITZ's volume fraction (or the increase of its thickness). When the type 3 ITZ is taken into consideration, the properties of the shale rocks reduce dramatically. This is because the type 3 has the lowest ITZ property values.

It can be concluded from the above that the quantitative effects of the ITZ on the material's macroscopic properties can be predicted by modifications to the three-phase sphere model using our proposed multiscale approach. And the thickness (which determines the ITZ volume fraction) and properties of the ITZ affect the properties of the equivalent inclusions greatly, which will lead to a decrease in the values of the shale rocks' properties when the ITZs are imperfect.

5.3 Discussion on the influence of the multi-inclusions

There are many components in shale rock, such as quartz, calcite and clays. From the viewpoint of our proposed multiscale framework, this implies that there are many types of inclusions in the porous matrix. The properties of the inclusions may influence the shale rock properties. For simplicity, the ITZ effects are not taken into consideration here.

Three types of inclusions, including quartz, calcite and dolomite, are employed as examples to illustrate their quantitative influence on the shale rock properties based on our proposed multiscale framework. The bulk modulus and shear modulus of quartz are 37.9GPa and 44.3GPa [15]. These two values are 77 GPa and 32 GPa, and 95 GPa and 45 GPa for the calcite and dolomite, respectively [54].

With these three types of inclusion, four different volume proportions are considered as examples, as shown in Table 2. The sum of volume fractions of these three types of inclusions is denoted by c_{t3}.

Figs. 6 (a)–(b) present the variations in the mechanical properties of the shale rock with different inclusions. The effective properties improve gradually with the increase of inclusions volume fractions. The dolomite seems to enhance the rock stiffness better than the other two inclusions, as it enjoys the highest properties.

Further, the influences of homogenization sequences are identified for different types of inclusions. Let's assume that the inclusions are only the calcite and dolomite. There are two homogenization sequences when our proposed multilevel homogenizations scheme is utilized. One is to perform the former and the latter homogenization with the calcite and the dolomite, respectively; the other is the opposite order. The volume ratios of these two inclusions are 10:1, 1:1 and 1:10 in this example.

Figs. 7(a)–(b) display the variations in the mechanical properties of the shale rocks with different inclusion volume fractions using two different homogenization sequences. It can be seen that the predicting results are very near to each other with different homogenization sequences when different inclusion volume proportions are considered.

In summary, the properties and volume fractions of the inclusions play an important role in the mechanical properties of the shale rock materials. However, the identifications show that there are no meaningful differences between the two predicting results using different homogenization sequences when our proposed multilevel homogenization schemes are performed.

6 Conclusions

This paper proposes a multiscale framework to quantitatively predict the transversely isotropic properties of shale rock with the multi-inclusion and ITZ effects. In the proposed framework, multiscale models are proposed to describe the shale rock microstructures from the nanoscale to the macroscale. A new multilevel micromechanical homogenization scheme is presented to quantitatively estimate the

transversely isotropic properties of shale rocks with the multi-inclusion and ITZ effects. The explicit form solutions for the transversely isotropic properties are obtained by utilizing the Hill polarization tensor without numerical integration and the standard tensorial basis. Moreover, our predicted results are compared with the available experimental data and predicting results of the existing model. The influences of the multi-inclusions and ITZs on the material's macroscopic properties are discussed using the proposed multiscale framework. From this study, the following main conclusions can be drawn:

(1) Comparisons with the available experimental data and the existing estimations show that our proposed multiscale framework is both feasible and capable of predicting the transversely isotropic properties of shale rock with the multi-inclusion and ITZ effects in an explicit form.

(2) With a better ITZ performance, the equivalent inclusions and the shale rock enjoy higher effective mechanical properties. When the properties of the ITZs are the same as those of their inclusions, results estimated by the existing model can be obtained by the developed framework.

(3) The volume fractions and properties of the multi-inclusions, such as quartz, calcite and dolomite, play important roles in determining the macroscopic properties of shale rocks. However, the homogenization sequences of different inclusions have little effects on our predicting results.

Acknowledgements

This work is supported by the Research Development Fund Programme of the University of Warwick, the National Key Basic Research and Development Programme (973 Programme, No. 2011CB013800). We would also like to express our gratitude to Prof. Woody Ju at UCLA and Prof. Zhiguo Yan at Tongji University for their kind help in this research.

Appendix A Properties of tensorial basis T

According to Levin and Markov [14], and Sevostianov et al. [20] the convenience of the tensorial basis is in the following properties:

1. If a general transversely isotropic symmetric fourth rank tensor $\mathbf{C}$ is expressed in the T-basis.

$$\mathbf{C} = C_1\mathbf{T}^2 + C_2\left(\mathbf{T}^1 - \frac{1}{2}\mathbf{T}^2\right) + C_3\mathbf{T}^3 + C_4\mathbf{T}^4 + C_5\mathbf{T}^5 + C_6\mathbf{T}^6 \tag{A1}$$

with

$$C_1 = \left(C_{1111} + C_{1122}\right)/2,\ \ C_2 = 2C_{1212},\ \ C_3 = C_{1133},\ \ C_4 = C_{3311},\ \ C_6 = C_{3333} \tag{A2}$$

the inverse tensor $\mathbf{C}^{-1}$ is determined by the expression

$$\mathbf{C}^{-1} = \frac{C_6}{2\Delta}\mathbf{T}^2 + \frac{1}{C_2}\left(\mathbf{T}^1 - \frac{1}{2}\mathbf{T}^2\right) - \frac{C_3}{\Delta}\mathbf{T}^3 - \frac{C_4}{\Delta}\mathbf{T}^4 + \frac{4}{C_5}\mathbf{T}^5 + \frac{2C_1}{\Delta}\mathbf{T}^6 \tag{A3}$$

where $\Delta = 2\left(C_1C_6 - C_3C_4\right)$.

2. If two tensors $\mathbf{C}$ and $\mathbf{D}$ are given in the T-basis, then the contraction of these tensors over two indices is defined as

$$\begin{aligned} C_{ijmn}D_{mnkl} = {} & \left(2C_1D_1 + C_3D_4\right)T^2_{ijkl} + C_2D_2\left(T^1_{ijkl} - \frac{1}{2}T^2_{ijkl}\right) + \left(2C_1D_3 + C_3D_6\right)T^3_{ijkl} \\ & + \left(2C_4D_1 + C_6D_4\right)T^4_{ijkl} + \frac{1}{2}C_5D_5T^5_{ijkl} + \left(C_6D_6 + 2C_4D_3\right)T^6_{ijkl} \end{aligned} \tag{A4}$$

References

[1] Thomsen L. Seismic anisotropy. Geophysics 2001; 66(1):40-41.

[2] Ulm FJ, Abousleiman Y. The nanogranular nature of shale. Acta Geotech 2006; 1(2):77-88.

[3] Dewhurst DN, Sarout J, Piane CD, Siggins AF, Raven MD. Empirical strength prediction for preserved shales. Mar Petrol Geol 2015; 67: 512–525.

[4] Farrokhrouz M, Asef RM, Kharrat R. Empirical estimation of uniaxial compressive strength of shale formations Geophysics, 2014; 79:D227-D233.

[5] Sayers CM. The elastic anisotropy of shales. J Geophys Res 1994; 99(B1): 767-774.

[6] Sayers CM. Stress-dependent seismic anisotropy of shales. Geophysics 1999; 64(1): 93-98.

[7] Sayers CM. Seismic anisotropy of shales. Geophys Prospect 2005; 53(5): 667-676.

[8] Chang C, Zoback MD, Khaksar A. Empirical relations between rock strength and physical properties in sedimentary rocks. J Petrol Sci Eng 2006; 51:223–237.

[9] Hornby BE, Schwartz LM, Hudson JA. Anisotropic effective-medium modeling of the elastic properties of shales. Geophysics 1994; 59(10): 1570-1583.

[10] Giraud A, Huynh QV, Hoxha D, Kondo D. Application of results on Eshelby tensor to the determination of effective poroelastic properties of anisotropic rocks-like composites. Int J Solids Struct 2007; 44(11-12): 3756-3772.

[11] Bayuk IO, Ammerman M, Chesnokov EM. Upscaling of elastic properties of anisotropic sedimentary rocks. Geophys J Int 2008; 172: 842-860.

[12] Bobko CP, Gathier B, Ortega JA, Ulm FJ, Borges L, Abousleiman YN. The nanogranular origin of friction and cohesion in shale-A strength homogenization approach to interpretation of nanoindentation results[J]. Int J Numer Anal Met 2011; 35: 1854-1876.

[13] Guo ZQ, Li XY, Liu C, Feng X, Shen Y. A shale rock physics model for analysis of brittleness index, mineralogy and porosity in the Barnett Shale. J Geophys Eng 2013; 10: 1-10.

[14] Levin VM, Markov MG. Elastic properties of inhomogeneous transversely isotropic rocks. Int J Solids Struct 2005; 42 (2): 393-408.

[15] Ortega JA, Ulm FJ, Abousleiman Y. The effect of the nanogranular nature of shale on their poroelastic properties. Acta Geotech 2007; 2(3): 155-182.

[16] Yanase K, Ju JW. Effective elastic moduli of spherical particle reinforced composites containing imperfect interfaces. Int J Damage Mech 2012; 21: 97-127.

[17] Nie SH, Basaran C. A micromechanical model for effective elastic properties of particulate composites with imperfect interfacial bonds. Int J Solids Struct 2005; 42,:4179-4191.

[18] Qu J. Eshelby tensor for an elastic inclusion with slightly weakened interface. J Appl Mech 1993; 60: 1048-1050.

[19] Qu J. The effect of slightly weakened interfaces on the overall elastic properties of composite materials. Mech Mater 1993; 14, 269-281.

[20] Sevostianov I, Yilmaz N, Kushch V, Levin V. Effective elastic properties of matrix composites with transversely-isotropic phases. Int J Solids Struct 2005; 42: 455-476.

[21] Ju JW, Chen TM. Micromechanics and effective moduli of elastic composites containing randomly dispersed ellipsoidal inhomogeneities. Acta Mech 1994; 103:103-121.

[22] Torquato S. Random heterogeneous materials: microstructure and macroscopic properties .Springer 2001.

[23] Eshelby JD. The determination of the elastic field of an ellipsoidal inclusion, and related problems. Proc R Soc London Ser A 1957; 241: 376-396.

[24] Eshelby J D. Elastic inclusions and inhomogeneities. In: Progress in solid mechanics. Amsterdam 1961.

[25] Eshelby JD. The elastic field outside an ellipsoidal inclusion. Proc R Soc London Ser A 1959; 252:561-569.

[26] Mura T. Micromechanics of Defects in Solids. Martinus Nijhoff Publishers, the Netherlands 1987.

[27] Mori T, Tanaka K. Average stress in matrix and average elastic energy of materials with misfitting inclusions. Acta Metall 1973; 21: 571-574.

[28] Benveniste Y. A new approach to the application of Mori-Tanaka's theory in composite materials. Mech Mater 1987; 6: 147-157.

[29] Hill R. A self-consistent mechanics of composite materials. J Mech Phys Solids 1965; 13: 213-222.

[30] Bobko CP, Ulm FJ. The nano-mechanical morphology of shale. Mech Mater 2008; 40: 318-337.

[31] Chen YY, Furmann A, Mastalerz M, Schimmelmann A. Quantitative analysis of shales by KBr-FTIR and micro-FTIR. Fuel 2014; 116: 538-549.

[32] Josh M, Esteban L, Delle Piane C, Sarout J, Dewhurst DN, Clennell MB. Laboratory characterisation of shale properties. J Petrol Sci Eng 2012; 88-89: 107-124.

[33] Chen YY, Mastalerz M, Schimmelmann A. Heterogeneity of shale documented by micro-FTIR and image analysis. J Microsc 2014; 256(3): 177-189.

[34] Ju JW, Chen TM. Effective elastic moduli of two-phase composites containing randomly dispersed spherical inhomogeneities. Acta Mech 1994; 103:123-144.

[35] Ju JW, Zhang XD. Micromechanics and effective transverse elastic moduli of composites with randomly located aligned circular fibers. Int J Solids Struct 1998; 35(9-10):941-960.

[36] Ju JW, Sun LZ. A novel formulation for the exterior-point Eshelby's tensor of an ellipsoidal inclusion. J Appl Mech 1999; 66(2):570-574.

[37] Ju JW, Sun LZ. Effective elastoplastic behavior of metal matrix composites containing randomly located aligned spheroidal inhomogeneities. Part I: micromechanics-based formulation. Int J Solids Struct 2001; 38(2):183-201.

[38] Sun LZ, Ju JW. Effective elastoplastic behavior of metal matrix composites containing randomly located aligned spheroidal inhomogeneities. Part II: applications. Int J Solids Struct 2001; 38(2):203-225.

[39] Sun LZ, Ju JW. Elastoplastic modeling of metal matrix composites containing randomly located and oriented spheroidal particles. J Appl Mech 2004; 71:774-785.

[40] Ju JW, Yanase K. Micromechanics and effective elastic moduli of particle-reinforced composites with near-field particle interactions. Acta Mech 2010; 215 (1):135-153.

[41] Ju JW, Yanase K. Micromechanical effective elastic moduli of continuous fiber-reinforced composites with near-field fiber interactions. Acta Mech 2011; 216 (1):87-103.

[42] Sheng P. Effective-medium theory of sedimentary rocks. Phys. Rev. B. 1990; 41:4507-4512.

[43] Zhu HH, Chen Q, Ju JW, Yan ZG, Guo F, Wang YQ, Jiang ZW, Zhou S, Wu B. Maximum entropy based stochastic micromechanical model for two-phase composite considering the inter-particle interaction effect [J]. Acta Mech, 2015; 226(9): 3069–3084.

[44] Zhu HH, Chen Q, Yan ZG, Ju JW, Zhou S. Micromechanical model for saturated concrete repaired by electrochemical deposition method. Mater Struct 2014; 47:1067-1082.

[45] Yan ZG, Chen Q, Zhu HH, Ju JW, Zhou S, Jiang ZW. A multiphase micromechanical model for unsaturated concrete repaired by electrochemical deposition method. Int J Solids Struct 2013; 50(24): 3875-3885.

[46] Chen Q, Zhu HH, Ju JW, Guo F, Wang LB, Yan ZG, Deng T, Zhou S. A stochastic micromechanical model for multiphase composite containing spherical inhomogeneities. Acta Mech 2015; 226(6):1861 – 1880.

[47] Chen Q, Zhu HH, Yan ZG, Deng T, Zhou S. Micro-scale description of the saturated concrete repaired by electrochemical deposition method based on Mori-Tanaka method (in Chinese). J Build Struct 2015; 36(1): 98-103.

[48] Chen Q, Zhu HH, Yan ZG, Ju JW, Deng T, Zhou S. Micro-scale description of the saturated concrete repaired by electrochemical deposition method based on self-consistent method(in Chinese). Chi J Theor and Appl Mech 2015; 47(2): 367-371.

[49] Yang QS, Tao X, Yang H. A stepping scheme for predicting effective properties of the multi-inclusion composites. Int J Eng Sci 2007; 45: 997-1006.

[50] Berryman JG. Long-wave propagation in composite elastic media II. Ellipsoidal inclusion. J Acoust Soc Am. 1980; 68(6): 1820-1831.

[51] Norris A. A differential scheme for the effective moduli of composites. Mech Mater 1985; 4(1):1-16.

[52] Christensen RM, Lo KH. Solutions for effective shear properties in three phase sphere and cylinder models. J Mech Phys Solids 1979; 27: 315-330.

[53] Withers PJ. The determination of the elastic field of an ellipsoidal inclusion in a transversely isotropic medium, and its relevance to composite materials. Philos Mag A 1989; 59 (4): 759-781.

[54] Mavko G, Mukerji T, Dovrkin J. The Rock Physics Handbook. Cambridge University Press, New York 2009.

Figures

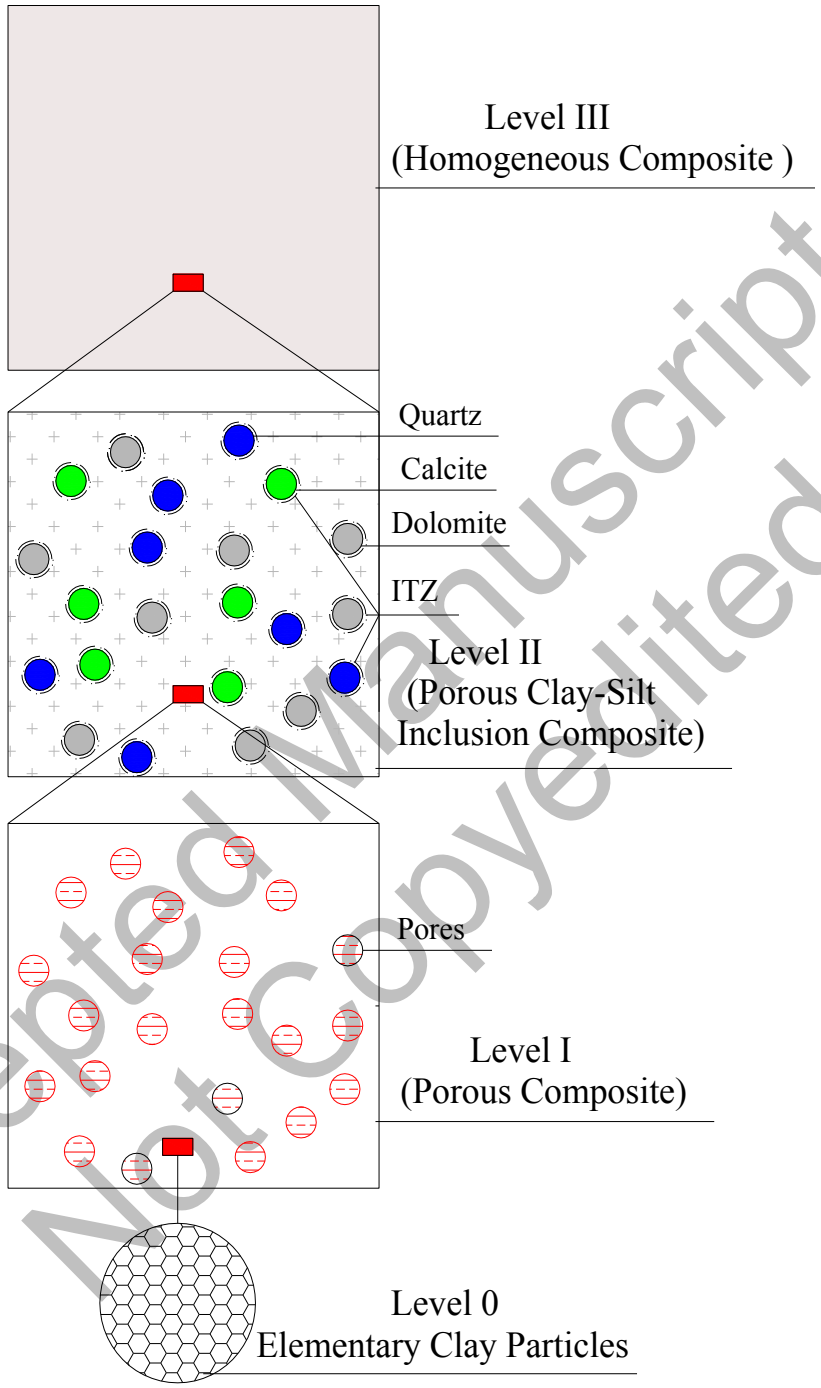

Fig. 1. The multiscale models for shale rocks with multi-inclusions and ITZs.

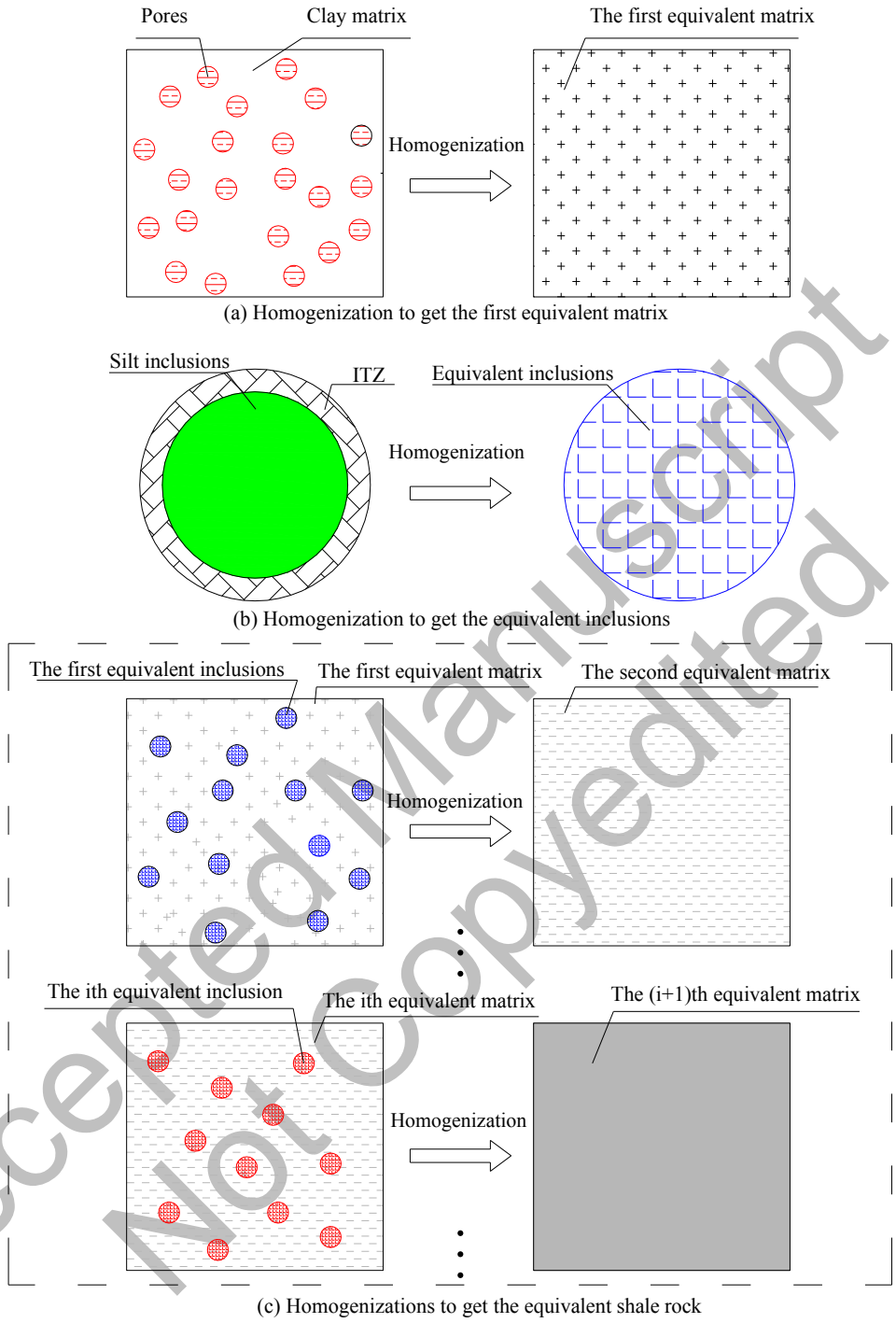

Fig. 2. A homogenization framework for the properties of the shale rock with multi-inclusions and ITZs, with i representing the type of the equivalent inclusion (i=1,2,…n, where n is the sum of all the inclusion types, and the (n+1)th equivalent matrix is the equivalent shale rock with multi-inclusions and ITZs)

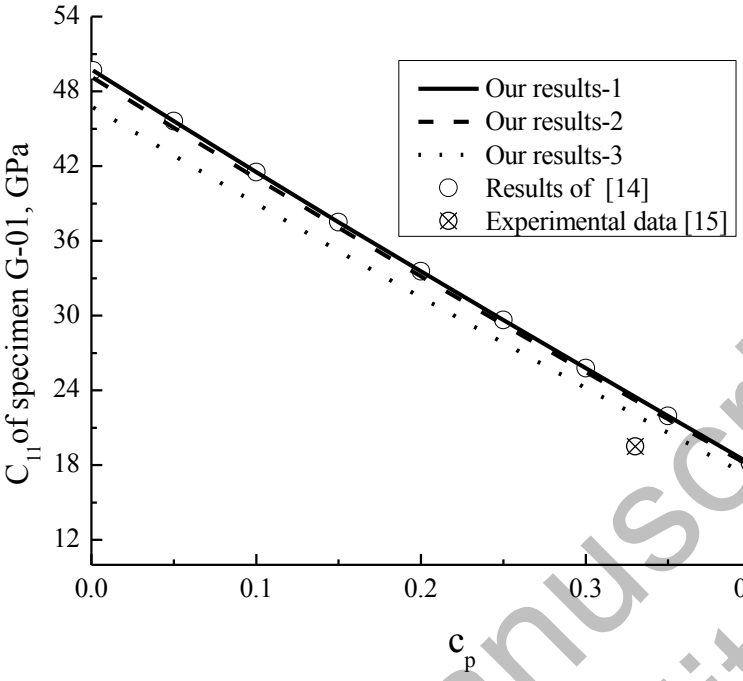

(a)

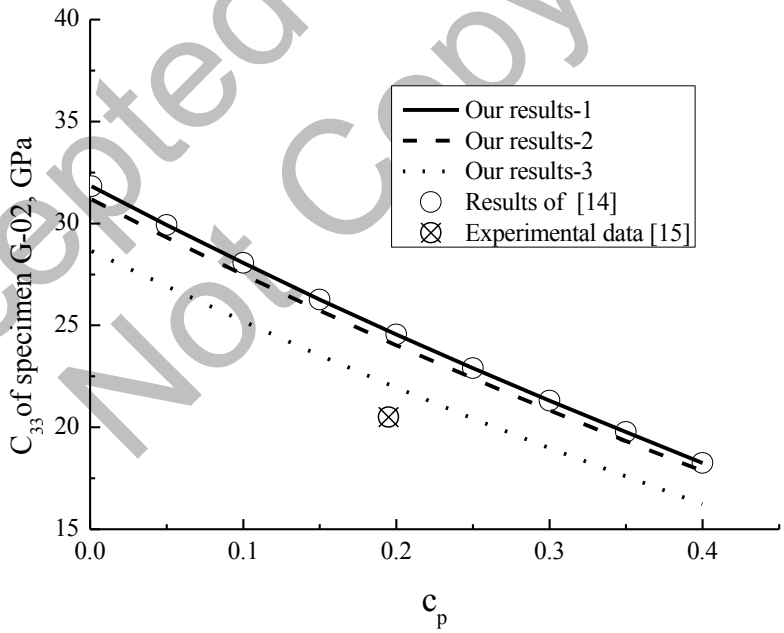

(b)

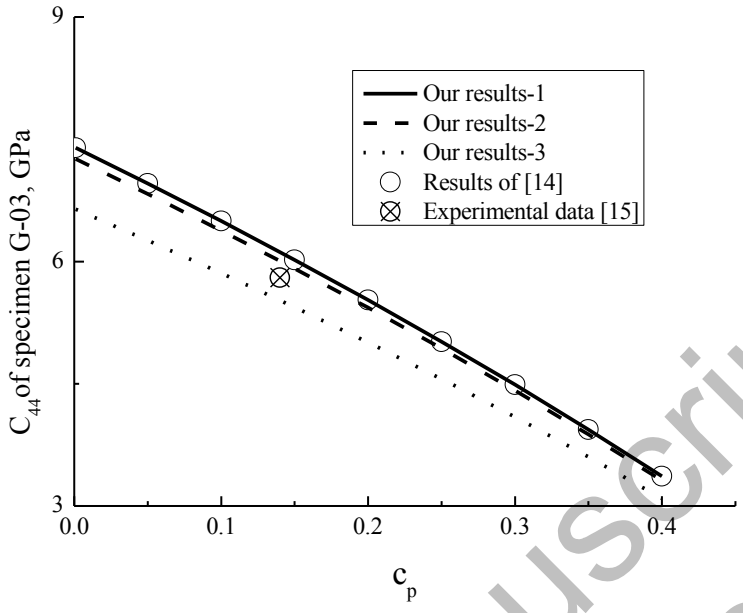

(c)

Fig. 3. Comparison of the effective properties among our predictions, the experimental data and the existing estimations, where -1,-2 and -3 represent predicting results using the first, second, and third types of ITZ properties, respectively; c_p denotes the volume fraction of the micro-pores in the porous clay composite.

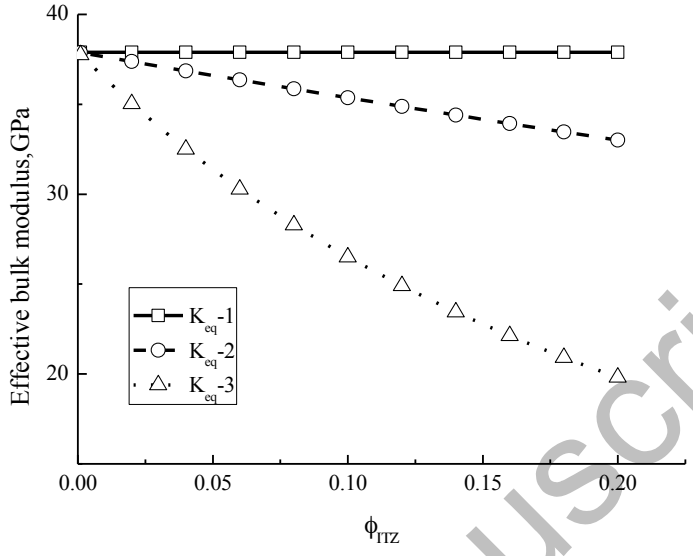

(a) The effective bulk modulus of the equivalent quartz inclusions denoted by K_{eq}

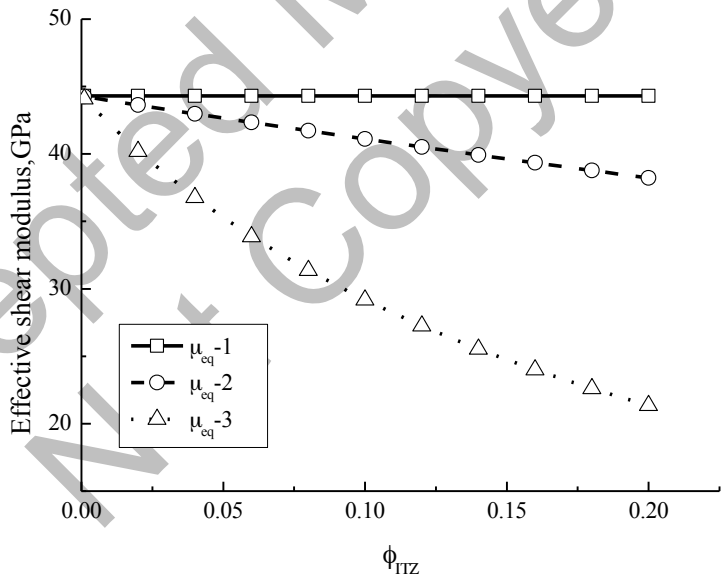

(b) The effective shear modulus of the equivalent quartz inclusions denoted by μ_{eq}

Fig. 4. The influence of different ITZs on the effective properties of the equivalent inclusions, where -1,-2 and -3 represent predicting results using the first, second, and third types of ITZ properties, respectively; ϕ_{ITZ} means the volume fraction of ITZ in the equivalent inclusions.

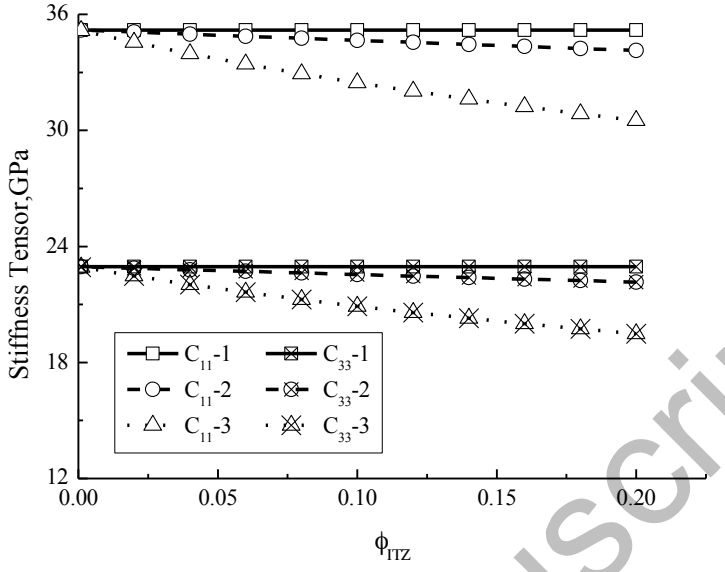

(a) C_{11} and C_{33}

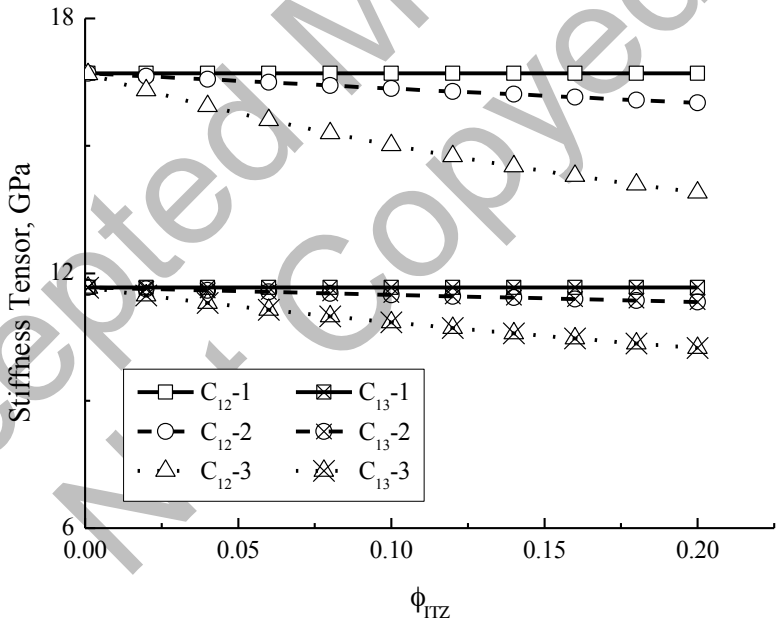

(b) C_{12} and C_{13}

Fig. 5. The influence of different ITZs on the effective properties of shale rocks, where -1,-2 and -3 represent predicting results using the first, second, and third types of ITZ properties, respectively; ϕ_{ITZ} means the volume fraction of ITZ in the equivalent inclusions.

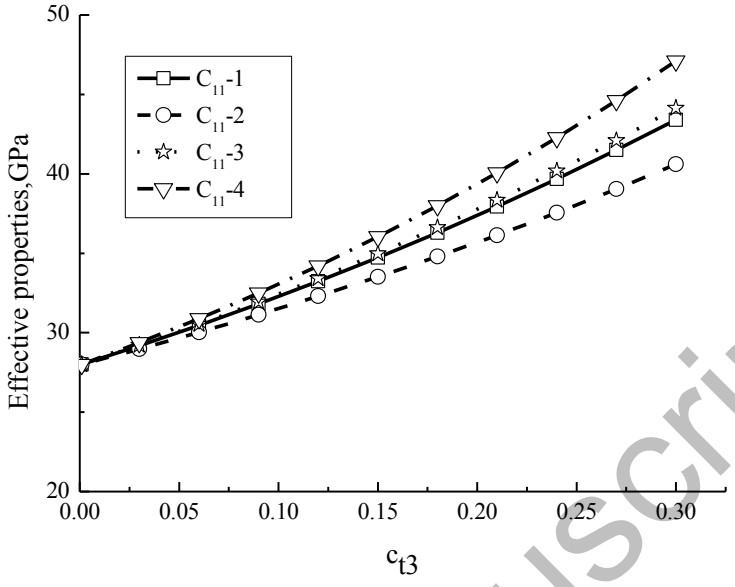

(a) C_{11}

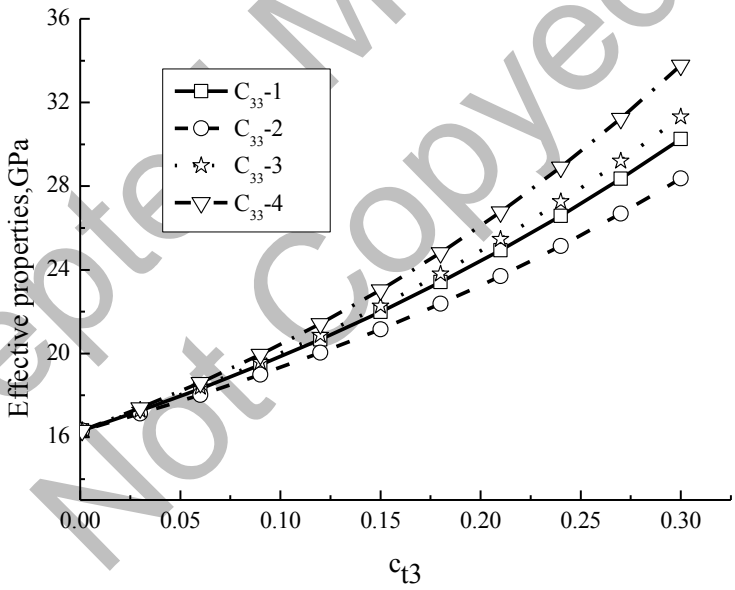

(b) C_{33}

Fig. 6. The influence of different inclusions on the effective properties of shale rocks, where -1,-2 ,-3 and -4 represent predicting results using the first, second, third and fourth types of volume proportions, respectively; c_{t3} denotes the sum of volume fractions of quartz, calcite and dolomite inclusions.

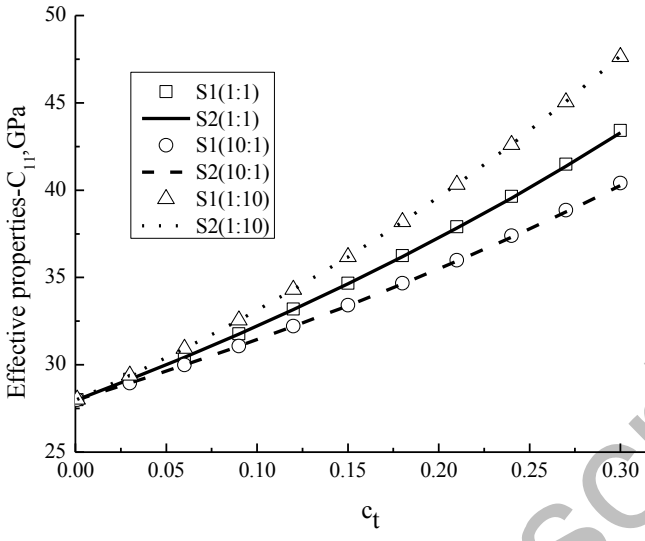

(a) C_{11}

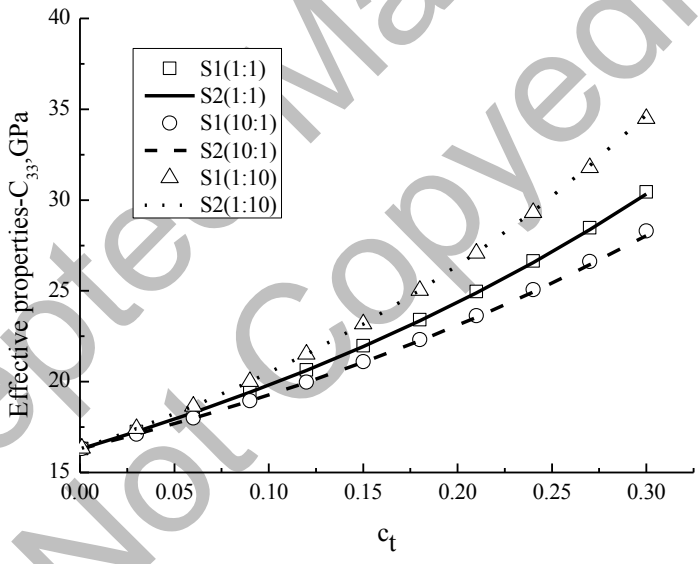

(b) C_{33}

Fig. 7. The influence of homogenization sequences on the effective properties of shale rocks, with S1 representing the first homogenization sequence which is to perform the former and the latter homogenizations with the calcite and the dolomite inclusions, respectively; with S2 representing the opposite sequence; with ratios in the bracket denoting the volume proportions between the calcite and the dolomite inclusions, c_t denotes the sum of volume fractions of calcite and dolomite inclusions

Table 1 Properties of ITZ between the quartz inclusion and matrix

	Bulk modulus (GPa)	Shear modulus (GPa)
Type 1	37.9	44.3
Type 2	37.9*0.5	44.3*0.5
Type 3	37.9*0.1	44.3*0.1

Table 2 The volume proportions for the three types of inclusions

	Quartz	Calcite	Dolomite
Proportion 1	1	1	1
Proportion 2	10	1	1
Proportion 3	1	10	1
Proportion 4	1	1	10